Clustering dynamics in globally coupled map lattices

Fagen Xie[1,2] and Gang Hu[1,3]
[1]*China Center of Advanced Science and Technology, (World Laboratory), P.O. Box 8730, Beijing, 100080, China*
[2]*Institute of Theoretical Physics, Academia Sinica, Beijing 100080, China*
[3]*Department of Physics, Beijing Normal University, Beijing 100875, China*
(Received 20 December 1996)

Clustering bifurcations are investigated by considering models of globally coupled map lattices. Typical classes of clustering bifurcations are revealed. The clustering bifurcation thresholds of the coupled system are closely related to the bifurcation structures of a single map. In particular, cluster-doubling bifurcation induced period-doubling bifurcations and clustering induced chaos are found. At the onset of an N-cluster state we always find uniform cell number distribution in the N clusters and uniform phase separations between these clusters. [S1063-651X(97)06908-0]

PACS number(s): 64.60.Ak, 05.45.+b

The investigation of globally coupled extended systems has attracted rapidly growing interest in recent years [1–6]. They arise naturally in studies of Josephson junctions arrays [1], multimode laser [2], charge-density wave [3], oscillatory neuronal systems [4], and so on. A number of intriguing and novel high-dimensional features have been revealed in these spatiotemporal systems. However, up to date, different types of clustering bifurcations have been treated individually, the general picture about the bifurcation structure and the common features at the onsets of the clustering bifurcations have not been considered. These structures and features are very important for the theoretical predictions and practical applications of clustering bifurcations. We take the following globally coupled map lattice (GCML)

$$x_{n+1}(i)=(1-\epsilon)f(x_n(i))+\frac{\epsilon}{L}\sum_{j=1}^{L} f(x_n(j)), \quad i=1,\ldots L, \tag{1}$$

as our main model, where n denotes the discrete time, i labels the lattice site with L system size. $f(x)$ prescribes the local dynamics, and is chosen as the logistic map $f(x)=ax(1-x)$. ϵ gives the long-range coupling strength. In Ref. [5], Kaneko presented the very rich and interesting behaviors of Eq. (1) for positive ϵ. Negative ϵ represents also many practical situations, such as antiferromagnetic coupling [6] and resistive coupling [1] and so on. Therefore, it is useful to unify the investigations of Eq. (1) for both positive and negative ϵ.

First, we consider clustering bifurcations from the simplest spatially homogeneous configuration, the so called *coherent* state. The stability of the state is easily calculated from the products of L-dimensional matrices for system (1) [5,7]. After simple algebra, the critical stability condition of this coherent state can be explicitly shown as

$$\epsilon_c=1-e^{-\lambda_0}, \tag{2}$$

where λ_0 is the Lyapunov exponent of the single logistic map [note, Eq. (2) is generally valid for any coherent state, whatever periodic or chaotic]. This critical stability boundary is shown in Fig. 1(a) with solid line. As $\epsilon>\epsilon_c$, the coherent state always exists, and is *locally* stable, while below the solid lines, the coherent state loses its stability and bifurcates to a multicluster state. From Eq. (2) it is clear that, coherent periodic motions are always stable for positive ϵ, they can lose stability only in the negative coupling regions. However, it should be emphasized that many attractors may coexist with the coherent state in the regime above the solid line for large system size L and large a.

A class of interesting states are multicluster states of uniform cell number distributions (i.e., $N_1=\cdots=N_k$, with N_i, being the number of the ith cluster), and in the case of periodic motion, each cluster may have the same motion except some uniformed distributed phase shifts. It will be shown that these kinds of states appear naturally at bifurcation thresholds. Afterwards, we focus on these kinds of states, and a period-m state with k clusters will be called the

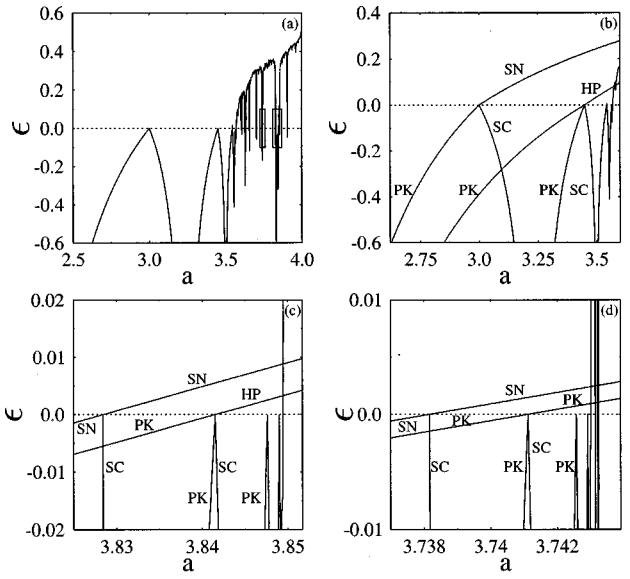

FIG. 1. Bifurcation figure for the homogeneous (coherent) state. Below the solid curves the homogeneous state loses its stability. (b) Clustering bifurcations in period-doubling region. SN, HB, PF, and SC represent the saddle-node, Hopf, pitchfork, and subcritical bifurcations, respectively. (c) The enlargement of the second rectangle of (a). The same as (b) where the period-three window is considered. (d) The enlargement of the first small rectangle of (a). The same as (c) where the period-five window is considered.

TmCk state. It often happens that $m=k$, the evolving dynamics of the TkCk state can be greatly reduced as

$$x_{n+1}=(1-\epsilon)f(x_n)+\frac{\epsilon}{k}\sum_{j=1}^{k} f(x_j), \tag{3}$$

where j indicates the cluster number which runs from 1 to k. For $k=2$, the solutions of Eq. (3) read

$$x_{1,2}=\frac{1+a-a\epsilon\pm\sqrt{(1+a-a\epsilon)^2-2(2-\epsilon)(1+a-a\epsilon)}}{2a(1-\epsilon)}. \tag{4}$$

The stability conditions of the TkCk state of Eq. (3) can be analytically given by computing the products of the Jacobi matrices of system (1). After some permutation and unitary transformation [7,8], the stability Jacobi matrix for Eq. (3) can be greatly simplified to a block-diagonal form as

$$J=\begin{pmatrix} \prod_{n=0}^{k} M_n & 0 \\ 0 & M' \end{pmatrix}, \tag{5}$$

where

$$M_n=\begin{pmatrix} \left(1-\frac{(k-1)\epsilon}{k}\right)f_n^1 & \frac{\epsilon}{k}f_n^2 & \cdots & \frac{\epsilon}{k}f_n^k \\ \frac{\epsilon}{k}f_n^1 & \left(1-\frac{(k-1)\epsilon}{k}\right)f_n^2 & \cdots & \frac{\epsilon}{k}f_n^k \\ \cdots & \cdots & \cdots & \\ \frac{\epsilon}{k}f_n^1 & \frac{\epsilon}{k}f_n^2 & \cdots & \left(1-\frac{(k-1)\epsilon}{k}\right)f_n^k \end{pmatrix},$$

with $f_n^i=ax_{n+i}(1-x_{n+i})$, $i=1,2,\ldots,k$, and $x_{n+k}=x_n$. $M'=(1-\epsilon)^k a^k \Pi_{n=0}^{k} x_n(1-x_n)\mathbf{I}$, $\mathbf{I}$ is the $(L-k)\times(L-k)$ unit matrix. Therefore, we obtain $L-k$ degenerate eigenvalues $\lambda=(1-\epsilon)^k a^k \Pi_{n=0}^{k} x_n(1-x_n)$, and other k eigenvalues. If the absolute values of all eigenvalues of J are less than *one*, the reference k-cluster state is stable. For $k=2$, the stability boundaries can be given explicitly. Increasing a from a small value, the T2C2 state appears from the spatially homogeneous state via saddle-node bifurcation and pitchfork bifurcation for $\epsilon>0$ and $\epsilon<0$, respectively, at the following critical thresholds:

$$a_c=1+\left(1+\frac{3}{(1-\epsilon)^2}\right)^{1/2}, \quad \epsilon>0,$$

$$a_c=2+\frac{1}{1-\epsilon}, \quad \epsilon<0 \tag{6}$$

and loses its stability via Hopf bifurcation and pitchfork bifurcation for $\epsilon>0$ and $\epsilon<0$, respectively, at

$$a_c=1+\left(1+\frac{5-3\epsilon}{(1-\epsilon)^2}\right)^{1/2}, \quad \epsilon>0,$$

$$a_c=1+\frac{\sqrt{2+(\epsilon-2)^2}}{1-\epsilon}, \quad \epsilon<0. \tag{7}$$

All these bifurcation lines and other clustering bifurcation lines in the period-doubling region are shown in Fig. 1(b). It is remarkable that in Fig. 1(b) one can find a clear rule to describe the entire clustering bifurcation structure in $\epsilon-a$ plane from the bifurcation sequence in the a axis at $\epsilon=0$. Actually, all bifurcation points for a single cell (at $\epsilon=0$) are multicodimensional bifurcation points in the $\epsilon-a$ parameter plane. The whole clustering bifurcation trees can grow up from this simple single cell bifurcation seeds. For $\epsilon>0$ one can find first order saddle-node bifurcation and second order Hopf bifurcation curves, while for $\epsilon<0$ one can find second order pitchfork bifurcation and first order subcritical bifurcation curves, all these bifurcation curves intersect with the a axis ($\epsilon=0$) at the critical points for single cell. These beautiful bifurcation trees can also be found in the chaos region associated with each periodic window. The enlarged regions of the rectangles in Fig. 1(a) for the bifurcations to three-cluster, and five-cluster states are shown in Figs. 1(c) and (d), respectively. The bifurcation figures are similar to Fig. 1(b), they are analytically predicted from Eqs. (1) and (5), and are fully verified by direct numerical computations. A difference of these figures from the two-cluster state is that for $\epsilon<0$ these multicluster states appear from chaotic motions via saddle-node bifurcation rather than pitchfork bifurcation.

To give clear pictures about the clustering bifurcations we show the asymptotic states of system (1) in Figs.2(a) and (b), where all stable homogeneous states are plotted by diamonds, stable multicluster states by solid lines, unstable states (both homogeneous and inhomogeneous) by dashed lines. The black regions in Fig. 2(a) represent stable quasiperiodic motion. In Fig. 2(a) we fix $\epsilon=0.2$, the system has only the coherent state below $a_c\approx 3.386$ (T1C1 for $a<3$ and T2C1 for $a>3$), the T2C2 state occurs via a saddle-node bifurcation at a_c, then the two states (T2C1 and T2C2) coexist in a certain a interval. As a continuously increases, the coherent state undergoes a series of period-doubling bifurcations leading to chaos, and then loses coherence at $a\approx 3.640$. The T2C2 state subjects to Hopf bifurcation at

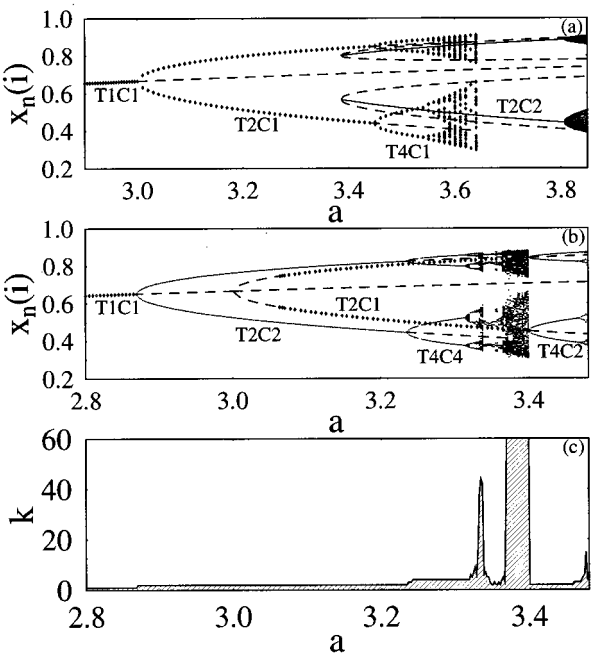

FIG. 2. Bifurcation sequences for certain couplings. Diamonds, solid lines, and dashed lines represent stable coherent states, stable multiple cluster states, and unstable states, respectively. (a) $\epsilon=0.2$, at $a\approx3.386$ a saddle-node bifurcation for two cluster state occurs. (b) $\epsilon=-0.15$, a cluster-doubling cascade induced period-doubling cascade leading to chaos is shown. (c) The number of cluster k plotted vs a with $\epsilon=-0.15$. In the region of clustering induced chaos k is of order L.

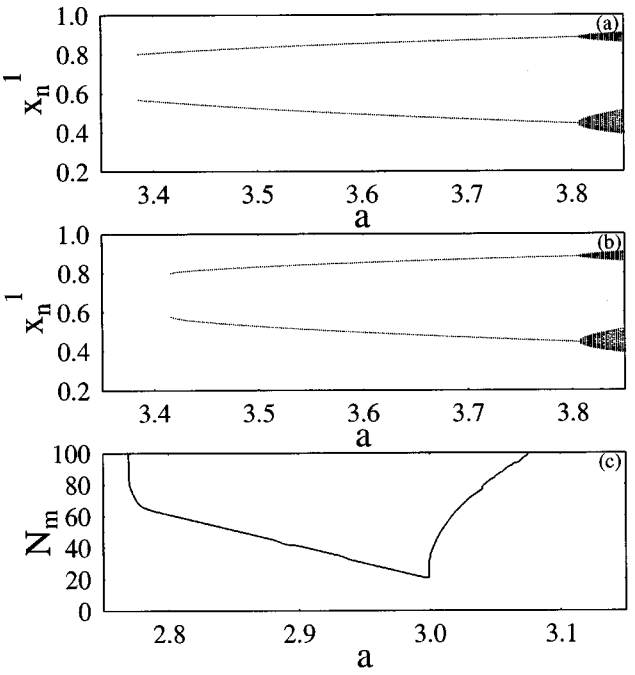

FIG. 3. T2C2 states for $L=200$. (a) $\epsilon=0.2$, $N_1=N_2=100$. (b) $\epsilon=0.2$, $N_1=98$, $N_2=102$. The T2C2 state appears much earlier in (a) than in (b). (c) $\epsilon=-0.3$, $L=200$. The number of the smallest site population N_m among possible N_1,N_2 plotted vs a. At the two bifurcation points N_m goes to $L/2$, indicating uniform cell number distribution.

$a\approx3.808$. In Fig. 2(b) we fix $\epsilon=-0.15$, the bifurcations are essentially different from those of Fig. 2(a). The T1C1 state first undergoes a cluster-period-doubling bifurcation at $a\approx2.870$ to create a stable T2C2 state. By increasing a, the state undergoes further cluster-period-doubling bifurcation and Hopf bifurcation leading to chaos. Figure 2(b) is extremely interesting due to the following novel features. First, we find a cluster-doubling induced period doubling. The value $a\approx2.870$ is far below the period-doubling condition for a single map. Global coupling leads to cluster doubling at this parameter, that induces period doubling in time. Second, we find a cluster-doubling sequence 1-2-4 (and the induced period-doubling sequence). We expect that this cluster-doubling cascade may proceed to a very large numbers of clusters. In our case this cascade is stopped at $k=4$ by Hopf bifurcation at $a\approx3.316$. Nevertheless, the tendency of cluster increasing bifurcations leading to chaos can be still seen in Fig. 2(c) for $a<3.4$, where we plot the number of clusters vs a for the states of Fig. 2(b). It is found in Fig. 2(b) that chaos can appear for $a<3.4$, where the nonlinear parameter a is far below the value for chaotic motion for the single map. At the same time in Fig. 2(c) we find the number of clusters diverges (to the order of L) in this chaos region. Then we conclude this chaos is made possible by clusterization, and as such is clustering induced chaos. It is remarkable that all analytical predictions in Fig. 1(b) are perfectly confirmed by numerical simulations of Eq. (1) in Fig. 2.

In the above we focused on the discussion of multiple cluster states with uniform cell number distributions. On one hand, these states can be easily treated by analyzing Eqs. (3) and that makes all predictions in Figs. 1 and 2 possible. On the other hand, these kinds of states appear generically and naturally under bifurcation conditions. We run Eqs. (1) from random initial conditions at $a=2.8$, then compute Eqs. (1) by gradually increasing a and by using the final state for the previous a as the initial state for the new a, we can surely get clusters with uniform cell number distributions for all cluster-doubling cascade.

Let us take a two-cluster state as an example. Usually, many two-cluster attractors with different N_1 and N_2 $(N_1+N_2=L)$ may coexist. However, at the onset of the two-cluster state we always first find the state with $N_1=N_2$ for even L, or $N_1=(L-1)/2$, $N_2=(L+1)/2$ for odd L. In Figs. 3(a) and (b) we fix $\epsilon=0.2$, $L=200$, and plot the two-cluster states for the occupation numbers $N_1=N_2=100$, and $N_1=98$, $N_2=102$, respectively. It is really striking that in Fig. 3(b) by slightly breaking the occupation balance the threshold for the two-cluster state is considerably raised. In Fig. 3(c) we fix $\epsilon=-0.3$, $L=200$, and plot N_m vs a, where N_m is the smallest occupation number among all possible N_1,N_2 for the two-cluster states of Eqs. (1). Small noises are added to the system sites for wiping out glass states with extremely small basins. It is interesting that N_m goes to $L/2$ at both left and right critical points (This phenomenon is also found by Kaneko for $\epsilon>0$ [5].)

Similar behavior happens also for general k-cluster bifurcations. In Figs. 4 we plot three-cluster states, arising via saddle-node bifurcation from spatiotemporal chaos. The three-cluster state with uniform cell number distribution arises much earlier than those with slight deviations from the uniform partitions for both $\epsilon>0$ and $\epsilon<0$. We have also examined many k-cluster bifurcations and always find the same behavior.

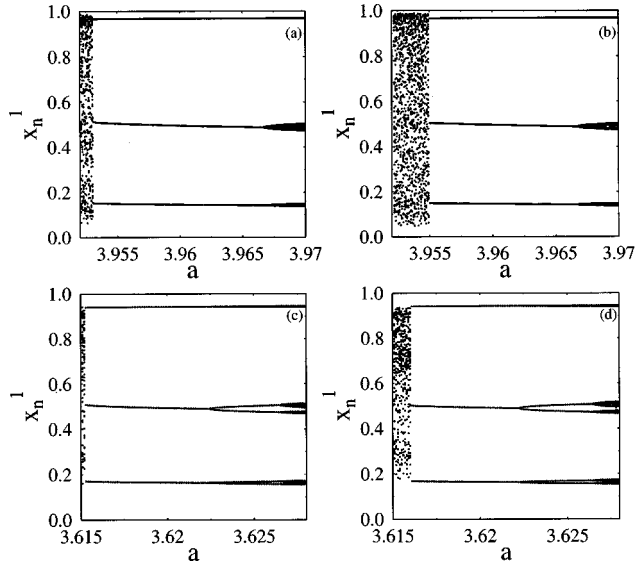

FIG. 4. Three-cluster states $L=300$. (a) $\epsilon=0.05$, $N_{1,2,3}=100$. (b) $\epsilon=0.05$, $N_1=98$, $N_2=100$, $N_3=102$. (c) $\epsilon=-0.1$, $N_{1,2,3}=100$. (d) (b) $\epsilon=-0.1$, $N_1=98$, $N_2=100$, $N_3=102$. At the onset of the three-cluster state one can only see the state with the uniform cell number distribution.

In this paper we took the globally coupled map lattices as our models. However, the ideas can be extended to more general globally coupled systems. We have examined globally coupled Josephson junctions and globally coupled Duffing oscillators, the clustering bifurcation features are qualitatively the same as those for the coupled map lattice systems. For instance, for the coupled Duffing oscillators

$$\dot{x}_i = y_i\,,$$

$$\dot{y}_i = 0.5 + f\,\cos t - x_i^3 - g(1+\epsilon)y_i + g\,\frac{\epsilon}{L}\sum_{j=1}^{L} y_j\,, \qquad (8)$$

where i labels the lattice site with L system size. We present numerical results of the clustering bifurcation tree structure in Fig. 5(a) and a clustering bifurcation sequence in Fig. 5(b), they are essentially the same as Figs. 1(a) and 2(b), respectively. Analytical results can also be conducted, they will appear in our full paper.

In this paper we systematically analyze the entire clustering bifurcation structure of globally coupled dynamic systems in parameter space. We find that the whole complicated clustering bifurcation tree can grow from the bifurcation sequence of a single cell, which are very well known in the study of low-dimensional systems. According to this tree structure we can well predict the bifurcations to very rich types of clusters. At the onset of the N-cluster state we always identify uniform cell number distribution in these N clusters, and uniform phase separations between these clusters. This feature is very useful for considerably simplifying the analytical treatment and it makes the explicit presentation of cluster bifurcation structure possible. Moreover, we find interesting cluster-doubling bifurcations (linked to the period-doubling bifurcations of a single cell at zero coupling) leading to chaos.

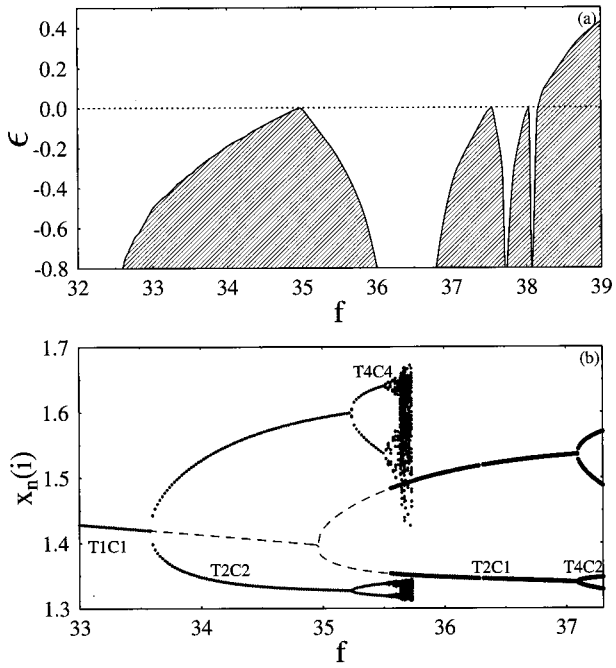

FIG. 5. (a) The same as Fig. 1(a) with Eqs. (8) simulated for $g=0.3$. In the shaded regions the coherent state is unstable due to the clustering bifurcations. (b) The same as Fig. 2(b) with Eq. (8) simulated for $g=0.3$ and $\epsilon=-0.3$. $x_n(i)$ is taken at $t_n=2\pi n$ after the transient process.

This work was supported by the National Natural Science foundation of China and the Project of Nonlinear Science.

[1] K. Wiesenfeld and P. Hadley, Phys. Rev. Lett. **62**, 1335 (1989); K. Y. Tsang and K. Wiesenfeld, Appl. Phys. Lett. **56**, 495 (1990); S. Watanabe and S. H. Strogatz, Phys. Rev. Lett. **70**, 2391 (1993); S. H. Strogatz and R. E. Mirollo, Phys. Rev. E **47**, 220 (1993); A. A. Chernikov and G. Schmidt, *ibid.* **52**, 3415 (1995); H. G. Winful and L. Rahman, Phys. Rev. Lett. **65**, 1575 (1990); K. Wiesenfeld and J. W. Swift, Phys. Rev. E **51**, 1020 (1995); D. Domínguez and H. A. Cerdeira, Phys. Rev. Lett. **71**, 3359 (1993); Phys. Rev. B **52**, 513 (1995).

[2] K. Wiesenfeld, C. Bracikowski, G. James, and R. Roy, Phys. Rev. Lett. **65**, 1749 (1990).

[3] H. Sompolinsky, D. Golomb, and D. Kleinfeld, Phys. Rev. A **43**, 6990 (1991).

[4] S. H. Strogatz, C. M. Marcus, R. M. Westervett, and R. E. Mirollo, Physica D **36**, 23 (1989).

[5] K. Kaneko, Phys. Rev. Lett. **63**, 219 (1989); **65**, 1391 (1989); Physica D **41**, 137 (1990); **54**, 5 (1991).

[6] M. Antoni and S. Ruffo, Phys. Rev. E **52**, 2361 (1995).

[7] Zhilin Qu *et al.*, Phys. Rev. E **49**, 1099 (1994).

[8] P. J. Davis, *Circulant Matrices* (Wiley, New York, 1979).